Journal of Aerosol Science 191 (2026) 106669

Contents lists available at ScienceDirect

Journal of Aerosol Science

journal homepage: www.elsevier.com/locate/jaerosci

Investigation of particle size-related artifacts in analyte quantification of particulate samples using infrared spectroscopy methods

Kabir Rishi [a], Orthodoxia Zervaki [a], Bon-Ki Ku [a], Nicholas Pugh [a,b], Chen Wang [a], Vasileia Vogiazi [a], Pramod Kulkarni [a,c,*]

[a] Centers for Disease Control and Prevention (CDC), National Institute for Occupational Safety and Health (NIOSH), Health Effects Laboratory Division (HELD), 1090 Tusculum Ave, Cincinnati, OH, 45226, USA
[b] South Dakota School of Mines & Technology, Department of Mechanical Engineering, 501 E St Joseph St, Rapid City, SD, 57701, USA
[c] University of Cincinnati, Department of Environmental and Public Health Sciences, College of Medicine, 160 Panzeca Way, Cincinnati, OH, 45267, USA

ARTICLE INFO

Handling Editor: Chris Hogan

Keywords:
Aerosol
Infrared spectroscopy
Lorenz-Mie scattering
Size-related artifacts

ABSTRACT

Infrared absorption spectroscopy is commonly used to quantify chemicals in the particulate phase for environmental and occupational aerosol exposure measurements. Unlike gas-phase analyte quantification, the analytical figures of merit depend on the characteristics of the particulate phase, in particular the aerosol size distribution. In the Mie scattering regime, where the particle size is comparable to the incident infrared wavelength, the bias in analyte quantification can depend on particle size. This error may depend on how well the size distribution of the aerosol matches with that of the reference material used to calibrate the method. While the impact of packing densities, and spectral interferences from the substrate and other minerals in the aerosol has been assessed in previous work, the impact of aerosol size distribution has not been explored. In this work, the Lorenz-Mie solution to Maxwell's equation was used to determine the bias in mass quantification of quartz in typical occupational aerosols for which the IR method is commonly used. Our experimental findings were benchmarked with the Lorenz-Mie solution using model spherical polystyrene particles. Practical deviations due to the asymmetric shape of quartz particles size-fractionated using different cascade impactors are presented and compared with literature studies on quartz aerosols. The expected bias in analyte quantification using different quartz standard reference materials relative to NIST SRM 1878a was assessed. The implications on quartz quantification due to differences in aerosol size distribution at different locations in the coal mine, granite quarries, and during construction activities such as stone finishing and grinding are presented and discussed.

1. Introduction

Infrared (IR) absorption spectroscopy is a non-destructive analytical technique commonly used for quantification of analytes in gas

* Corresponding author. Centers for Disease Control and Prevention (CDC), National Institute for Occupational Safety and Health (NIOSH), Health Effects Laboratory Division (HELD), 1090 Tusculum Ave, Cincinnati, OH, 45226, USA.
E-mail address: pramod.kulkarni@uc.edu (P. Kulkarni).

https://doi.org/10.1016/j.jaerosci.2025.106669
Received 22 May 2025; Received in revised form 13 August 2025; Accepted 14 August 2025
Available online 27 August 2025
0021-8502/Published by Elsevier Ltd.

and particulate phase. For exposure assessment and health effects studies of aerosols that involve quantitation of airborne contaminants, infrared methods offer robust and cost-effective solutions. Infrared methods have been widely used for quantification of respirable crystalline silica (RCS), such as quartz, in aerosols from coal mines (Bandopadhyay, 2010; Dodgson & Whittaker, 1973; Larsen et al., 1972), construction sites (Chisholm, 1999; Rappaport et al., 2003; Virji et al., 2002), granite quarries (Cares et al., 1973), and gold mines (Verma et al., 1992). Exposure to RCS puts workers at a greater risk of developing silicosis, lung cancer, non-malignant respiratory diseases, and kidney disease (Merchant et al., 1986; OSHA, 2016; Rice et al., 2002).

Absorption of infrared radiation at specific resonant frequencies vibrates the molecular bonds in the analyte of interest, resulting in a characteristic absorption spectrum. Application of infrared methods to gases or liquid samples is straightforward, where spectroscopically measured absorption is calibrated using known reference gas concentration. However, application of IR to measurement of particulate samples requires that IR absorption signal be calibrated using the known gravimetric mass of a standard reference material (SRM) (ASTM, 2014; MSHA, 2013; NIOSH, 2017a, 2017b). Furthermore, characteristics of the particulate samples, particularly particle size in relation to wavelength, play an important role. For wavelength-sized particles (Mie regime, typically for diameters larger than 4.1 μm for quartz particles), scattering becomes a significant contribution to the infrared extinction spectra. This scattering manifests as slanted baseline in non-absorbing spectral regions that can superimpose and distort the absorption bands. Since analyte quantification is based on the extinction (the sum of absorption and scattering), and scattering is strongly dependent on particle size, the inferred absorbance (from extinction measurement) of the analyte will be influenced by the particle size. Larger particles will scatter more light, leading to an increase in extinction that may not be directly related to absorption by the analyte, thus complicating quantification based on absorption.

For many aerosol contaminants of interest to environmental or occupational exposure assessment, the aerosol size distribution, particularly in the respirable fraction, can be different from that of the SRM used for calibration. This difference can lead to an underestimation or overestimation of the analyte mass concentration. Such differences can contribute to a significant degree to the overall measurement uncertainty, particularly when measuring at trace concentrations, e.g. when quantifying concentrations below the permissible exposure limit for RCS of 50 $\mu g/m^3$ (8-h time-weighted average) (OSHA, 2016).

Various studies have empirically demonstrated that for quartz containing aerosols (approximately >1 μm), the IR extinction (ε, or absorption for weakly-scattering particles) decreases with increasing particle size (Bhaskar et al., 1994; Dodgson & Whittaker, 1973; Foster & Walker, 1984; Harrick & Riederman, 1965; Kauffer et al., 2002; Page, 2003; Sato et al., 1969; Stacey et al., 2009; Tuddenham & Lyon, 1960; Udvardi et al., 2017). It has been hypothesized that a reduction in particle crystallinity (Dempster & Ritchie, 1952; Gordon & Harris, 1955; Koopmans & Rieck, 1965; Nagelschmidt et al., 1952) during communition of SRMs, results in a decrease in IR extinction with decreasing particle size for sub-micron (<1 μm) quartz particles (Foster & Walker, 1984; Page, 2003). The IR extinction can be calculated using the Lorenz-Mie theory ($\varepsilon_{\mathrm{Mie}}$) (Mie, 1908), over a wide aerosol size range. The Lorenz-Mie theory describes the scattering and absorption efficiencies (Q_{sca}, Q_{abs}) of an incident electromagnetic plane wave (of wavelength, λ) by a homogenous spherical material of size, d_{p}, with a known complex refractive index, $m = \mathrm{n} + i\mathrm{k}$, (n is real, k is imaginary). The total extinction efficiency, $Q_{\mathrm{ext}} = Q_{\mathrm{abs}} + Q_{\mathrm{sca}}$, is directly related to the measured IR transmittance, T (Lukacs et al., 2015). Based on Beer-Lambert's law, the measured (or experimental) extinction, $\varepsilon_{\mathrm{exp}} = -\ln_{10}(T)$, accounts for both scattering and absorption from particles. Although strictly valid for a single spherical particle (diameter, d_{p}) with cross sectional area of $\pi {d_{\mathrm{p}}}^2/4$, the Lorenz-Mie solution can be extended to a number/count-based particle size distribution, $n(d_{\mathrm{p}})$, comprising of total number of particles, N_{T}, by integrating $Q_{\mathrm{ext}}(d_{\mathrm{p}}, \lambda, m)$ over a size distribution such that the calculated IR extinction, $\varepsilon_{\mathrm{Mie}}$ (Sumlin et al., 2018), is given by,

$$\varepsilon_{\mathrm{Mie}} = \left(\frac{1}{\ln 10 A_{\mathrm{dep}}}\right) \int_0^{\infty} \left(\frac{\pi {d_{\mathrm{p}}}^2}{4}\right) Q_{\mathrm{ext}}(d_{\mathrm{p}}, \lambda, m) n(d_{\mathrm{p}}) \mathrm{d}d_{\mathrm{p}} \tag{1}$$

Equation (1) assumes that each aerosol particle in the distribution scatters independently of each other (i.e., no multiple scattering) (Brewster & Tien, 1982; Drolen & Tien, 1987; Hottel et al., 1971; Hunt & Logan, 1972). In equation (1), $n(d_{\mathrm{p}}) = N_{\mathrm{T}} \mathrm{f}(d_{\mathrm{p}})$, such that $\mathrm{f}(d_{\mathrm{p}})$ represents a frequency distribution for example, Gaussian (normal) or Log-normal. The latter is generally used to specify an aerosol size distribution. A_{dep} refers to the sample deposition area on the filter. Under the assumption of uniform packing density, A_{dep} can be considered instead of the detector area. For spherical particles, N_{T} can be estimated from the measured gravimetric mass, M_{T}, on the filter such that,

$$M_{\mathrm{T}} = \int_0^{\infty} \left(\frac{\pi {d_{\mathrm{p}}}^3}{6}\right) n(d_{\mathrm{p}}) \mathrm{d}d_{\mathrm{p}} = N_{\mathrm{T}} \int_0^{\infty} \left(\frac{\pi {d_{\mathrm{p}}}^3}{6}\right) \mathrm{f}(d_{\mathrm{p}}) \mathrm{d}d_{\mathrm{p}} \tag{2}$$

The objective of this study was to investigate the bias in analyte quantification, using the IR transmittance measurements based on equation (1) above, due to differences in particle size of sample and SRM. Specifically, we examined: (i) the applicability of equation (1) for predicting the measured IR extinction, $\varepsilon_{\mathrm{exp}}$ (using instrumental setup commonly used for quartz quantification), for a model system of monodisperse, spherical polystyrene particles, (ii) deviations from Lorenz-Mie theory for polydisperse, non-spherical quartz particles, and (iii) the expected bias in mass/concentration quantification based on the calibration curves used in IR analytical methods due to differences in particle size distribution between quartz SRMs and occupationally-relevant crystalline silica aerosols.

2. Experimental

2.1. Materials

Aqueous solutions of NIST-traceable spherical polystyrene microspheres (Duke Standards, ThermoFisher Scientific) with diameters ranging from 0.4 μm to 10 μm and density of 1.05 g/cm^3 were used as is.

Quartz SRM 1878, SRM 1878b powders (National Institute of Standards and Technology, NIST, Gaithersburg, MD) were aerosolized (see details in the following section) and size-fractionated using either Andersen cascade impactor (ACI; Model 20–800, Tisch Environmental, Atlanta, GA), or a Micro-orifice Uniform Deposit Impactor (MOUDI; Model 110-R, TSI Inc., Shoreview, MN). The ACI has eight stages with cut-sizes equal to 9 μm, 5.8 μm, 4.7 μm, 3.3 μm, 2.1 μm, 1.1 μm, 0.7 μm, and 0.4 μm when operated at 28.3 lpm, while the MOUDI has ten stages with cut-sizes equal to 18 μm (pre-cut), 10 μm, 5.6 μm, 3.2 μm, 1.8 μm, 1.0 μm, 0.56 μm, 0.32 μm, 0.18 μm, 0.10 μm, 0.056 μm when operated at 30 lpm. For each stage, 50 % of particles greater than the cut-size are collected while 50 % of particles smaller than the cut-size cascade through.

Four types of filter media with a diameter of 25 mm, Polyvinylchloride/PVC membranes (5 μm pore size, SKC Inc.), Polytetrafluoroethylene/PTFE membranes with a support ring (3 μm pore size, SKC Inc), Versapor® acrylic copolymer membranes (0.8 μm pore size, Pall Corporation), and Polycarbonate/PC membranes (0.8 μm pore, SKC Inc) were used.

2.2. Particle collection

Aqueous suspensions of the NIST-traceable aqueous polystyrene size standards at various concentrations were prepared using particle-free water (UHPLC-UV grade, Fisher Chemical). The diluted suspensions were sonicated for 2 min before vacuum filtration onto different filter media (A_{dep} of 0.7–2.01 cm^2) described previously.

A stock suspension of 0.22 g of SRM 1878 in 200 ml of water (UHPLC-UV grade) was nebulized using clean compressed air. The aerosolized droplets passed through a diffusion dryer and subsequently drawn into the ACI using a pump operated at 28.3 lpm. Dry powder of SRM 1878b was aerosolized using the vortex shaking method (Ku et al., 2013) and sampled using the MOUDI operated at 30 lpm. The flow rate through the cascade impactors was verified using a mass flowmeter (Model 4043H, TSI Inc) before each collection. A standard HEPA filter (PN 12144, Pall Corporation) was connected at the pump's outlet. The size-fractionated SRM 1878 collections on each impaction stage were rinsed with water, while the SRM 1878b collections were rinsed with 2-propanol (A461–212, Optima LC/MS grade, Fisher Scientific). These particulate suspensions were sonicated in an ultrasonic cleaner (FS60D, Fisher brand) for 20 min and subsequently deposited on to PVC membranes (A_{dep} of 1.54 cm^2) using vacuum filtration.

2.3. Gravimetric measurements

Filter media were conditioned for 24 h inside a humidity-controlled chamber prior to weighing. Following sample deposition, filter media were dried at 30–40 °C inside a muffle furnace (550-128, Fisher Scientific) for 2–4 h and returned to the humidity-controlled chamber to condition. Pre- and post-gravimetric measurements were performed on either a 7-digit microbalance (XPR6U, Mettler Toledo) or a 6-digit microbalance (AT20, Mettler Toledo). Each filter was pre- and post-weighed in three replicate measurements and the difference of the averages was used to calculate the measured gravimetric mass, M_T.

2.4. Fourier transform infrared spectroscopy (FT-IR) measurements

The IR transmittance, T, (average of three) for each sample was measured using a FT-IR instrument equipped with a filter measurement attachment (Model Alpha-II, Bruker Corporation, Billerica, MA). T was converted to the measured IR extinction, $\varepsilon_{exp} = -\ln_{10}(T)$. Each measurement was averaged over 32 scans for wavenumbers ranging from 400 to 4000 cm^{-1} at a resolution of 2 cm^{-1}. Background signal from blank filters was measured and subsequently subtracted from the sample signal. Linear baselines were constructed between 680 and 720 cm^{-1} for polystyrene samples, and between 770 and 815 cm^{-1} for quartz samples (MSHA, 2013). After baseline correction, the peak height at 698 cm^{-1} was used as the ε_{exp} for polystyrene. The spectral peaks at 698 cm^{-1} and 756 cm^{-1} are associated with the out-of-plane bending vibration mode of the C-H (Hanssen and Zhu, 2002; Jung et al., 2018). While quartz shows vibration modes at 780 cm^{-1} and 800 cm^{-1} and the peak at 800 cm^{-1} is typically considered in analytical methods (Madsen et al., 1995), we used the peak height at 780 cm^{-1} to represent ε_{exp}. This peak is unique to quartz among the crystalline silica polymorphs and amorphous silica (Kischkat et al., 2012; NIOSH, 2017a, 2017b; Steyer et al., 1974).

2.5. Optical and scanning electron microscopy

PSL particles of different sizes on PTFE filter media were imaged using a confocal Raman microscope (Model XploRA PLUS, HORIBA Instruments Inc., Irvine, CA) operated using the LabSpec 6 software. PTFE filters offered better optical contrast compared to PVC and PVDF. For polystyrene spheres >2 μm in size, an objective lens (Model MPlan N 10×, 0.25 NA, ∞/–/FN22, Olympus/Evident Scientific, Waltham, MA) was used. For the 1 μm spheres, an objective lens (MPlan N 5×, 0.10 NA, ∞/–/FN22, Olympus/Evident Scientific, Waltham, MA) was used. Mosaic images were taken to image the entire deposition area on the filter media.

Size-fractionated quartz particles from the bottom four stages (d_{50} ranging from 0.4 to 2.1 μm) of the ACI were vacuum filtered through PC filters. These samples were analyzed on a desktop scanning electron microscope (SEM; Phenom XL, Thermo Fisher

Scientific, Waltham, MA) in the low-pressure mode (~1 Pa) at 15 kV acceleration voltage and 1.7 nA probe current with a back-scattered electron detector. Micrographs were obtained at a magnification of about 5000×. The images were processed and analyzed by image analysis software (MIPAR Image Analysis, version 3.4.0, Columbus, OH) to determine particle size distribution based on projected area (Sosa et al., 2014).

3. Results & discussion

3.1. Lorenz-Mie calculations

Plots for Q_{ext} as a function of particle size, d_p, were obtained using a numerical code (MATLAB, MathWorks, Inc., Nattick, MA). This numerical code (Bohren & Huffman, 2008; Mätzler, 2002) uses the size parameter, $x = \pi d_p/\lambda$, as an input variable. For polystyrene, the average n_{PS}, and k_{PS} values (Myers et al., 2018) at λ (for 698.6 ± 2 cm^{-1}) were used. Since the optical properties of quartz are equal in two orthogonal directions (ordinary ray) and differ in the third orthogonal direction (extra-ordinary ray) (Di Biagio et al., 2014; He et al., 2019; Hudson et al., 2008; Longtin et al., 1988; Peterson & Weinman, 1969; Reed et al., 2017; Saksena, 1940, 1958; Šimon & McMahon, 1953; Spitzer & Kleinman, 1961), n_Q, and k_Q were estimated using the optical constants averaging (OCA) method such that, $n_Q = 2/3n_{Q,o} + 1/3n_{Q,eo}$ and $k_Q = 2/3k_{Q,o} + 1/3k_{Q,eo}$ (Di Biagio et al., 2014; Hudson et al., 2008; Peterson & Weinman, 1969; Reed et al., 2017). A similar spectral averaging (SA) method has also been proposed wherein $\varepsilon_{Mie} = 2/3\varepsilon_{Mie,o} + 1/3\varepsilon_{Mie,eo}$ (Hudson et al., 2008). The average $n_{Q,o}$, $k_{Q,o}$, $n_{Q,eo}$, and $k_{Q,eo}$ values (Reed et al., 2017; Spitzer & Kleinman, 1961) at λ (for 780.7 ± 2 cm^{-1}) were used. These values have been verified through emission spectroscopy on quartz crystals (Wenrich & Christensen, 1996). For Lorenz-Mie calculations, air was considered as the ambient medium since background signal from the filter media was subtracted during measurements. The refractive index for humid air in the mid-IR wavelength range is approximately 1.000273 (Mathar, 2007; Rank & Shearer, 1954), although the values differ in the visible and near infrared range (Ciddor, 1996). For simplicity, the refractive index of air was considered as 1.

3.2. Comparison of measured IR transmittance and theoretical IR extinction for model polystyrene spheres

Model polystyrene spheres were used to validate our instrumental setup used to measure IR transmittance of particulate samples collected on filter substrates. To calculate ε_{Mie}, particles on filter media with mean particle size, d_p, were considered to be normally distributed with a standard deviation of σ as listed in Table S1 in SI. A comparison of ε_{exp} and ε_{Mie} at 698 ± 2 cm^{-1} for polystyrene spheres over a wide range of sizes, d_p (or x, defined in the preceding section) and packing densities (M_T/A_{dep}) is shown in Fig. 1 (also plotted as $\varepsilon_{exp}/\varepsilon_{Mie}$ as a function of M_T/A_{dep} in Fig. S1 in SI). For x less than 1 (d_p < 4.6 μm for PSL particles) and packing density below 500 μg/cm^2 (solid red circles), ε_{exp} and ε_{Mie} deviate by 20 % at most (i.e., 20 % on each side of the 1:1 line), as indicated by the shaded region in Fig. 1. This agreement is well within the experimental uncertainty from many sources, including dependent scattering due to close packing or agglomerated particles. Particle agglomeration or clustering observed in the optical micrographs that span the filter deposition area (see Fig. S2 in the SI), is unavoidable during sample preparation and can contribute to measurement uncertainty of ε_{exp}.

For x greater than 1 (d_p > 4.6 μm for PSL particles) and packing density below 500 μg/cm^2 (solid blue circles), ε_{exp} and ε_{Mie} deviate

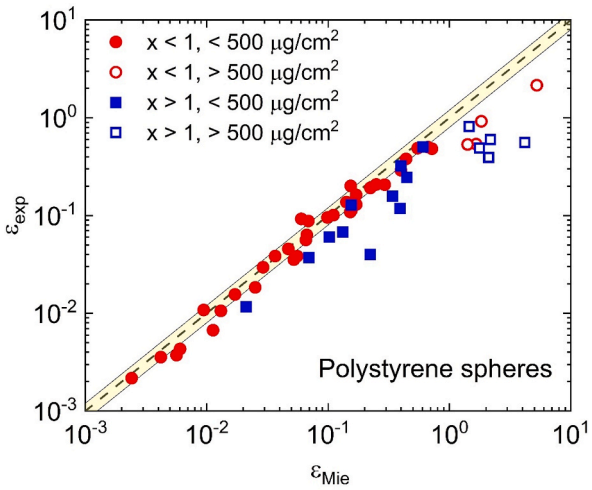

Fig. 1. Comparison of measured (ε_{exp}, and calculated (ε_{Mie} extinction for model polystyrene spheres with size parameters, x < 1 or d_p < 4.6 μm (red circles), and x > 1 (blue squares), and packing densities <500 μg/cm^2 (solid symbols), and >500 μg/cm^2 (open symbols). The yellow shaded region depicts a 20 % deviation on each side of the 1:1 line. (For interpretation of the references to colour in this figure legend, the reader is referred to the Web version of this article.)

further. Note that the differences might appear to be less exacerbated since the data is plotted on a log-scale. For particle circumference comparable to or greater than the incident wavelength, scattering contributes more to the total extinction in compared to absorption, resulting in poorer agreement between ε_{exp} and ε_{Mie}. For packing densities >500 μg/cm^2 (open red and blue circles), multiple or dependent scattering effects due to mutual interaction between particles are further exacerbated. To account for these interactions in packed fluidized beds, various frameworks such as the packed-sphere model (Cartigny et al., 1986; Yamada et al., 1986), gas model (Cartigny et al., 1986; Yamada et al., 1986), modified liquid model (Drolen & Tien, 1987; Smith & Henderson, 1970), and Percus-Yevick model (Drolen & Tien, 1987; Ishimaru & Kuga, 1982; Twersky, 1978; Wertheim, 1963), have been employed for $x < 1$. For $x > 1$, we refer the reader to another photometric model (Hapke, 2012). While the correction factors based on these models have been used in atmospheric sciences wherein particulate aerosols are suspended in gas/liquid, a direct application of these models to particulate laden filters is beyond the scope of this study.

3.3. Comparison of measured IR transmittance and theoretical IR extinction for non-spherical quartz

Since the Lorenz-Mie solution is applicable to spherical particles only, log-normal distributions specified by number-based volume equivalent diameter, d_{ve}^c, and geometric standard deviation, σ_g (Dunbar & Mitchell, 2005; Marple et al., 1991), for the size-fractionated quartz particles collected using the ACI/MOUDI impactors (see Table S2 in the SI) were considered for the calculations. A comparison of ε_{exp} and ε_{Mie} at 780 ± 2 cm^{-1} for quartz particles with x less than 1 ($d_{ve}^c < 4.1$ μm) and packing density below 500 μg/cm^2, fractionated using the ACI (SRM 1878; open and solid red squares) and MOUDI (SRM 1878b; solid blue circles) is shown in Fig. 2. Due to the non-spherical shape of the quartz particles, a 40 % deviation (i.e., 40 % on each side of the 1:1 line) indicated by the yellow shaded region between ε_{exp} and ε_{Mie} was considered. To account for the particle asymmetry, distributions of ellipsoids (Hudson et al., 2008), and spheroids (Reed et al., 2017) have been considered. While a significant improvement in peak fitting at 1100 cm^{-1} was observed by considering non-spherical shapes, no considerable difference was observed in the 770–815 cm^{-1} range (Reed et al., 2017).

For coarser particles in SRM 1878, there was a significant measurement bias introduced due to sampling and measurement artifacts; for example, for quartz particles on the upper stages of ACI (open red squares), the deviations extend beyond the shaded region in Fig. 2. Here the assumption of a unimodal size distribution was not invalid as confirmed by the SEM micrographs and corresponding distribution of projected area of the particles shown in Fig. S3 in SI. A multi-modal distribution of particles on the stages of cascade impactors has previously been observed (Bartz et al., 1979; Dekeyser & Dams, 1990; Dzubay & Hasan, 1990; SRM 1878 quartz particles were generated via nebulization in this study. The size of atomized water droplets depends on the flow rate (McCallion et al., 1996), such that lower flow rates result in bigger water droplets. Although a diffusion dryer was used, a reduction in efficiency could result in insufficient drying of water droplets; thus, large droplets containing small silica particles could be erroneously deposited on the upper stages of the cascade impactor resulting in multi-modal size distributions.

ε_{exp} for size-fractionated quartz particles ($x < 1$) from several literature studies (Dodgson & Whittaker, 1973; Foster & Walker, 1984; Kauffer et al., 2002; Stacey et al., 2009; Tuddenham & Lyon, 1960) was also compared with ε_{Mie} in Fig. 2 (open black symbols). Estimates of d_{ve}^c from the reported sizes, and σ_g are detailed in Table S3 in SI. No information pertaining to M_T, A_{dep}, baseline correction, and correction factors for determining ε_{exp} was available for data reported in the literature. For a given literature dataset, ε_{Mie} was scaled to the highest reported ε_{exp} by varying M_T/A_{dep}. The same M_T/A_{dep} was used to compute the remaining ε_{Mie} values for each reported d_{ve}^c. The calculated ε_{Mie} and ε_{exp} deviate by 40 % at most (i.e., 40 % on each side of the 1:1 line), demonstrating the

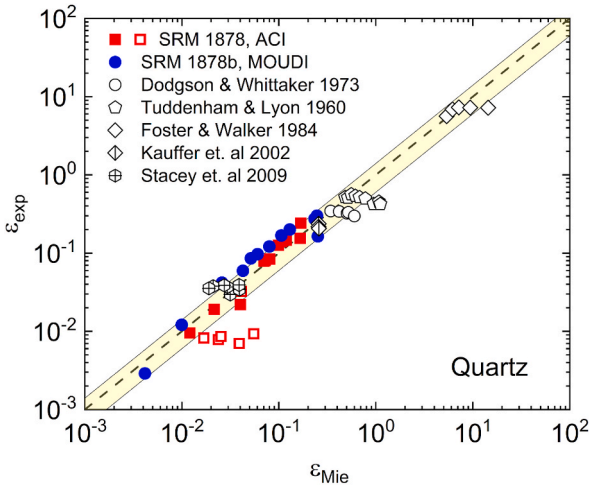

Fig. 2. Comparison of ε_{exp} and ε_{Mie} for quartz particles with size parameters, $x < 1$ (or $d_{ve}^c < 4.1$ μm) and packing densities <500 μg/cm^2, size-fractionated using ACI (open and solid red squares) and MOUDI (solid blue circles). The yellow shaded region depicts 40 % deviation on each side of the 1:1 line between ε_{exp} and ε_{Mie}. Comparison of ε_{exp} and ε_{Mie} literature data is also presented (open black symbols). (For interpretation of the references to colour in this figure legend, the reader is referred to the Web version of this article.)

applicability of the Lorenz-Mie solution to previous literature studies.

3.4. Quantification bias due to differences in particle size distributions of quartz standards used for calibration

In order to understand the extent of bias (b) introduced by differences in size distribution between sampled aerosols and the SRM, we performed Lorenz-Mie calculations. The bias was calculated by obtaining the difference in the total particulate mass, M_T, for a known size distribution of the sampled aerosol using equation (2) and the mass obtained from the SRM calibration curve, M_{cal} by calculating the ε_{Mie} using equation (1) for the same size distribution such that, $b = |M_{cal}(\varepsilon_{Mie}) - M_T|/M_T \times 100$. Here, M_{cal} can be estimated from the ratio of ε_{Mie} to the slope of a SRM calibration curve.

The calibration curve for different SRMs (constructed using Lorenz-Mie calculations) is shown in Fig. 3. For each reference material, the log-normal size distribution parameters, d^c_{ve}, and σ_g, estimated from literature (Stacey et al., 2009) are reported in Table S4 in SI. For each reference material, N_T was varied to obtain ε_{Mie}, and the calibration mass, M_{cal}, from equation (1), and (2), respectively.

The bias (b) in mass quantification due to differences in particle size distributions of the quartz aerosol and the SRM 1878a (certificate) calibration curve is shown in Fig. 4. It was assumed that the quartz aerosols were 100 % crystalline (equal to calibration standard). Fig. 4 reveals that the bias in mass quantitation is <40 % across all d^c_{ve} provided $\sigma_g < 1.6$. Similarly, for $d^c_{ve} < 2$ μm and all σ_g, the bias was under 40 %. For larger $d^c_{ve} > 3$ μm, and $\sigma_g > 2$, the bias in mass quantitation can range between 40 and 100 %, with greater biases at large d^c_{ve} and σ_g.

Fig. 4 also compares the bias in mass quantification for different quartz standards in use today. Owing to differences in origin and preparation methodology, their particle size distributions vary significantly. d^c_{ve} and σ_g for these standards were obtained from literature (Stacey et al., 2009; Verma & Shaw, 2001) as detailed in Table S4 in SI. It was assumed that all standards were 100 % crystalline, and Fig. 4 demonstrates the bias in mass quantification between the quartz reference materials purely based on differences in size distribution. In Fig. 4, d^c_{ve} and σ_g values for SRM 1878, Min-U-Sil 5, and A9950 (or Sikron F600) from both literature references listed in Table S4 in SI were considered (Stacey et al., 2009; Verma & Shaw, 2001). Quartz reference materials such as Quin 1 (Institut National de Recherche et de Sécurité in France), A9950 (Health and Safety Laboratory, U.K.), SRM 1878a (National Institute of Standards and Technology, USA), A9950 (AUST) No 1 (Australian National University and Deakin University, Australia), and DQ12 Bergbau (British Case Iron Research Association, U.K.) have <20 % quantification bias due to differences in size distribution relative to SRM 1878a (certificate). The bias in mass quantification increases to 20–40 % for SRM 1878 (National Institute of Standards and Technology, USA), Ottawa Silica Sand (Elliott Lake Laboratory, Canada), and A9950 (if d^c_{ve} and σ_g values from Verma and Shaw (2001) in Table S4 in SI is considered). However, the use of respirable fractions of Quin 1 and A9950, DQ12 (Health and Safety Laboratory, U.K.), and Min-U-Sil 5 increases the bias to 40–60 %, while the highly polydisperse ($\sigma_g \approx 3$) DQ12 Robock (British Case Iron Research Association, U.K.) shows ~ 80 % bias in mass quantification relative to SRM 1878a (certificate).

3.5. Quantification bias due to differences in particle size distribution for occupationally relevant, mixed aerosol exposures

The bias calculations discussed above assume 100 % crystalline content, whereas most real-world workplace aerosols show crystalline content between approximately 10–90 %. The range of parameters investigated for mixed aerosol exposures are detailed in Table 1. Occupational aerosols are complex, heterogenous mixtures of inorganic species (salts, minerals, metals), and carbonaceous compounds (Song et al., 2022). For example, aerosols from coal mines comprise of minerals such as calcite, quartz, dolomite, kaolinite, and illite in addition to carbonaceous coal dust (Pan et al., 2021; Riley et al., 2012), while aerosols generated during engineered stone

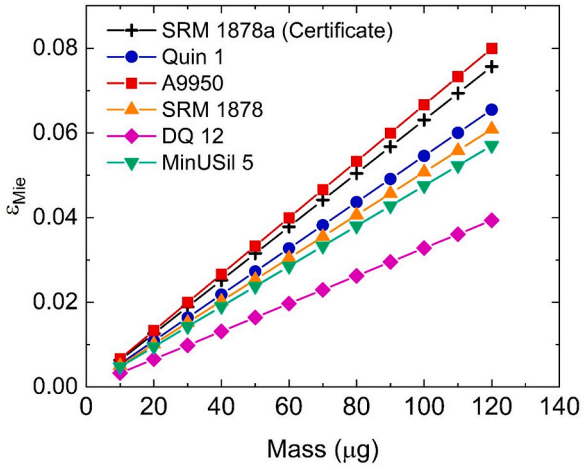

Fig. 3. Calculated calibration curve (ε_{Mie} vs the calibration mass, M_{cal}) based on the cumulative size distribution reported in quartz SRM 1878a (certificate) (Stacey et al., 2009). The slopes from linear regressions were 6.66×10^{-4}/μg (A9950), 6.31×10^{-4}/μg (SRM 1878a), 5.46×10^{-4}/μg (Quin 1), 5.07×10^{-4}/μg (SRM 1878), 4.75×10^{-4}/μg (Min-U-Sil 5), and 3.28×10^{-4}/μg (DQ 12).

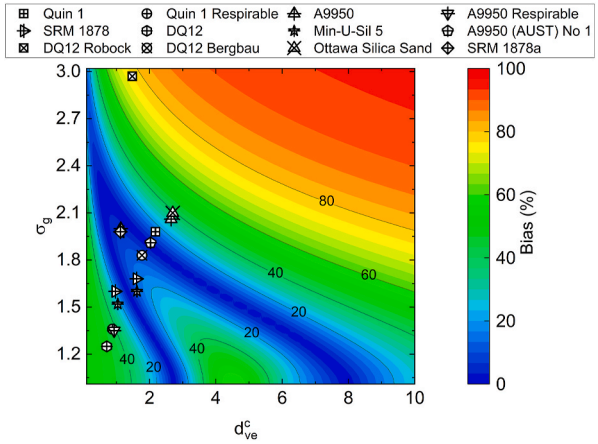

Fig. 4. A plot showing the bias in mass quantification of quartz particles (100 % crystallinity) with different log-normal size distributions relative to SRM 1878a (certificate). Bias in mass quantification for other available quartz reference materials relative to the SRM 1878a is also shown (d^c_{ve} and σ_g values for these reference materials listed in Table S4 in SI).

Table 1
Range of values for different parameters used for estimating the measurement bias in mass estimation from Lorenz-Mie calculations and actual mass for a given size distribution.

Parameter	Range of values investigated
Size distribution	Lognormal, d^c_{ve} = 0.1–10 μm, σ_g = 1.1–3
Morphology[a] (i.e. non sphericity)	Dynamic shape factor = 1.36 for quartz (1 for spheres)
Packing density[b]	3–432 μg/cm^2
Chemical composition (by volume)	Coal mine dust (46 % dolomite, 16 % calcite, 15 % kaolin, 14 % illite, 8 % quartz)
	Concrete/Cement dust (49 % dolomite, 32 % quartz, 19 % calcite)
	Granite quarry dust (73 % quartz, 18 % Al_2O_3, 9 % Fe_2O_3
	Engineered stone dust (93 % quartz, 7 % resin)

[a] Other values of dynamic shape factors were not explicitly tested, but different dynamic shape factors would result in different d^c_{ve} estimated from d^m_a, essentially impacting the size distribution.

[b] While the packing density range listed in the table (<500 μg/cm^2) was used to determine the feasibility of Lorenz-Mie calculations against experimental measurements for quartz in Fig. 2, the bias in mass aerosol mass (or concentration), $b = |M_{cal}(\varepsilon_{Mie}) - M_T|/M_T \times 100$, is independent of packing density, since both ε_{Mie} and M_T are directly related to the total number of particles, N_T, per equations (1) and (2), respectively.

fabrication show an abundance of quartz and polymer resin binder particles (Ramkissoon et al., 2022; Rishi et al., 2024; Thompson & Qi, 2023). Typical composition of coal mine dust (averaged from four locations within the mine) was 59.3 % coal, 17.7 % dolomite, 6.6 % calcite, 6.4 % kaolinite, 5.4 % illite, and 3.3 % quartz by mass (Pan et al., 2021). Similarly, for construction aerosols such as concrete dusts comprise of 45.1 % dolomite, 32.2 % quartz, and 18.3 % calcite by mass (Gharpure et al., 2021), while dusts released during engineered stone fabrication (averaged over 12 stones) comprise of 87 % quartz, and about 13 % resin binder by mass (Ramkissoon et al., 2023). On the contrary, dust from fabrication of natural stones such as granite comprises of 70 % quartz, 11 % Al_2O_3, and 5 % Fe_2O_3 by mass (Silva et al., 2023). These differences in the composition manifest as a change in refractive index of the aerosol for infrared spectroscopic measurements and calculations.

To compute bias in Fig. 5, a linear volume average mixing rule was used to determine the refractive indices (Hand & Kreidenweis, 2002; Hänel, 1968; Hasan & Dzubay, 1983; Liu & Daum, 2008; Lowenthal et al., 2000; Ouimette & Flagan, 1982) of mining and construction dusts. The refractive indices and densities of the constituents are listed in Table S5 in SI (Ashraf et al., 2019; Jäger et al., 2003; Polyanskiy, 2024; Querry, 1985, 1987). Fig. 5 shows the impact of varying quartz content (determined using SRM 1878a-based calibration shown in Fig. 3) in the workplace aerosols on quartz mass quantification for different aerosols with varying sampled aerosol size distribution parameters d^c_{ve}, and σ_g. The bias was determined as mentioned in the preceding section. It can be seen that the bias in mass quantification for engineered stone dust is similar to Fig. 4 since the quartz content is relatively high and the resin binder absorbs weakly at 780 cm^{-1} (see small k value in Table S5 in SI). Although counterintuitive, a marked reduction in the bias was observed for natural stone dusts such as granite. This was attributed to the strong absorption of Al_2O_3 at 780 cm^{-1} (see large k value in Table S5 in SI). For the same aerosol size distribution, a lower quartz content in the dust (such as 8 %, and 32 % of the total mineral composition in coal mine dust, and concrete/cement dust, respectively) results in a higher bias in mass quantification.

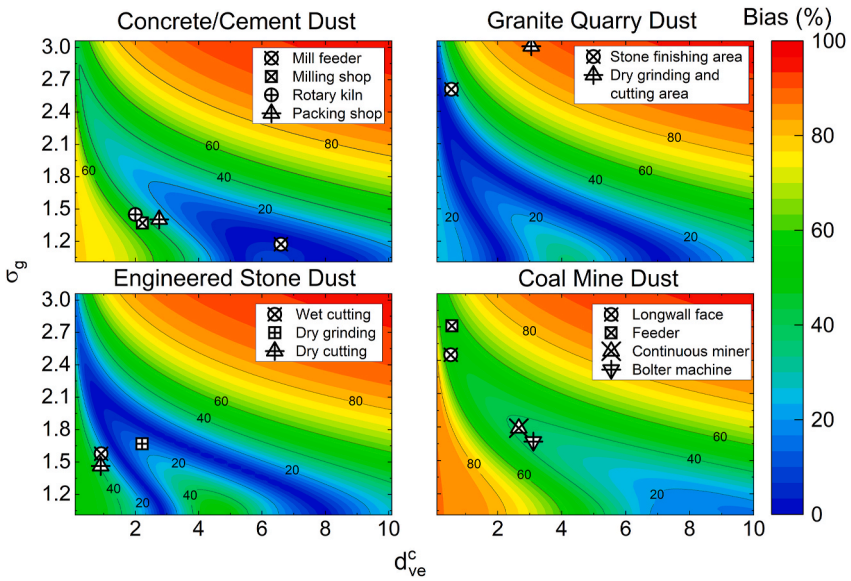

Fig. 5. A plot showing the bias in mass quantification for quartz in occupational aerosols such as concrete/cement dust (32.2 % quartz), granite quarry dust (70 % quartz), engineered stone dust (87 % quartz), and coal mine dust (8 % quartz of the mineral dust) with different log-normal size distributions relative to SRM 1878a (certificate). Bias associated with sampling at different sampling locations in the coal mine (Wang et al., 2024), granite quarry (Sirianni et al., 2008), and concrete/cement production facility (Menzelintseva et al., 2019). Bias in analyte mass quantification during different construction activities on engineered stones (Pavan et al., 2016; Thompson & Qi, 2023) is also shown (see Table S6 in SI for associated d_{ve}^{c} and σ_g values).

Fig. 5 shows practical size distributions of aerosols (Menzelintseva et al., 2019; Pavan et al., 2016; Sirianni et al., 2008; Thompson & Qi, 2023; Wang et al., 2024) (see Table S6 in SI) sampled at different locations in the workplace and the associated bias in quartz quantification using IR spectroscopic methods. For example, sampling dust near the mill feeder at a concrete/cement production facility (Menzelintseva et al., 2019), shows <20 % bias in analyte mass quantification. Sampling of concrete/cement dust in the packing shop shows a 20–40 % measurement bias, which increases to >40 % while sampling in the milling shop and near the rotary kiln. Sampling dusts in the stone finishing area in a granite quarry (Sirianni et al., 2008) also show a 20–40 % bias in analyte mass quantification, which increases to > 80 % due to a more polydisperse size distribution with larger modal diameter when sampled in the grinding and cutting areas. Similarly, sampling coal mine dust (Wang et al., 2024) near the continuous miner and bolter machine shows a 20–40 % bias in analyte mass quantification, which increases to 40–60 % when sampled near the feeder and longwall face. Construction activities such as grinding (Thompson & Qi, 2023) and cutting (Pavan et al., 2016) of engineered stone generate different particle size distributions relative to the calibration standard and consequently result in differing bias in analyte mass quantification.

4. Conclusions

Measured and calculated extinction efficiency (ε_{exp} and ε_{Mie}) for model PSL particles agreed within ±20 % for x less than 1 (d_p < 4.6 μm) and packing density below 500 μg/cm^2. Nonideal conditions, such as particle agglomeration, matrix effects from the sample substrate, and dependent scattering likely contributed to the observed difference. For x greater than 1 (d_p > 4.6 μm) scattering dominated absorption, while at packing densities >500 μg/cm^2 dependent scattering was significant, resulting in larger deviations between ε_{exp} and ε_{Mie}. Measured and calculated extinction efficiency (ε_{exp} and ε_{Mie}) for quartz particles agreed within ±40 % due to the asymmetric particle morphology. The estimated bias, based on ε_{Mie} calculated from the Lorenz-Mie theory is applicable for x less than 1 (i.e., d_{ve}^{c} < 4.1 μm for quartz containing aerosols), and packing densities <500 μg/cm^2 based on our experimental findings. This translates to a filter mass loadings of approximately 2 mg, and 4 mg on standard 25 mm, and 37 mm filters used for air sampling. The bias plots can be used up to a maximum air concentration of 2 mg/m^3 for a typical 8-h sampling period at 2 lpm for sampling using a 25 mm filter which is above the permissible exposure limit for RCS of 50 μg/m^3.

The bias in mass quantification for aerosols with very high (nearly 100 %) crystalline silica content (for example, engineered stone countertops) varies depending on the particle size distribution of quartz reference materials in use today worldwide. The bias is <20 % for Quin 1, A9950, A9950 (AUST) No 1 and DQ12 Bergbau relative to SRM 1878a. On the contrary, respirable fractions of Quin 1 and A9950, DQ12, and Min-U-Sil 5 showed a 40–60 % bias relative to SRM 1878a based on Lorenz-Mie calculations.

Occupational exposures comprise mixed aerosols with crystalline silica fractions ranging from 8 % in coal mine dust to about 87 % in dust from grinding of engineered stone countertops. Exposure assessment at different locations in coal mines, granite quarries, and concrete cement production facilities, or during different construction activities using IR spectroscopic methods result in analyte mass quantification bias relative to the calibration standard due to differences in particle size distributions as well. Moderate differences

between the particle size distributions of the sampled aerosol (for example, stone finishing area in a granite quarry, powder handling in concrete/cement production facility, continuous miner and bolter machine in coal mines) and the calibration SRM result in a 20–40 % bias in analyte mass quantification. When the modal diameter and polydispersity of the sampled aerosol (for example, grinding and cutting areas in granite quarry) is significantly higher than the calibration SRM, the bias in analyte mass quantification can exceed 80 %. The study highlights artifacts in IR measurement of workplace aerosols and the need to exercise caution when comparing different quantification methods.

CRediT authorship contribution statement

Kabir Rishi: Writing – review & editing, Writing – original draft, Visualization, Methodology, Investigation, Formal analysis, Data curation. **Orthodoxia Zervaki:** Visualization, Validation, Formal analysis. **Bon-Ki Ku:** Methodology, Investigation. **Nicholas Pugh:** Validation. **Chen Wang:** Investigation. **Vasileia Vogiazi:** Investigation. **Pramod Kulkarni:** Writing – review & editing, Supervision, Resources, Project administration, Conceptualization.

Disclaimer

The findings and conclusions in this report are those of the author(s) and do not necessarily represent the official position of the National Institute for Occupational Safety and Health (NIOSH), Centers for Disease Control and Prevention (CDC). The mention of any company or product does not constitute an endorsement by NIOSH/CDC.

Ethics approval

Activity was determined to meet the definition of research as defined in 46.102(l) but did not involve human subjects as defined in 46.103(e)(1).

Funding

This work was funded by the National Institute for Occupational Safety and Health through the National Occupational Research Agenda (NORA) grant (CAN 9390G1Y).

Declaration of competing interest

The authors declare that they have no known competing financial interests or personal relationships that could have appeared to influence the work reported in this paper.

List of Symbols

Symbol	Description
ε	IR extinction
$\varepsilon_{\mathrm{Mie}}$	IR extinction calculated from Lorenz-Mie theory
Q_{sca}	Scattering efficiency from Lorenz-Mie theory
Q_{abs}	Absorption efficiency from Lorenz-Mie theory
T	Measured IR transmittance
$\varepsilon_{\mathrm{exp}}$	Measured IR extinction, $\varepsilon_{\mathrm{exp}} = -\ln_{10}(T)$
d_{p}	Particle diameter (spherical morphology)
$n(d_{\mathrm{p}})$	Number-based size distribution
N_{T}	Total number of particles in a distribution
λ	Incident IR wavelength, inversely related to the wavenumber
m	Complex refractive index of the particles, $m = \mathrm{n} + i\mathrm{k}$, where n is real part while k is the imaginary part
$Q_{\mathrm{ext}}(d_{\mathrm{p}}, \lambda, m)$	Total extinction efficiency from Lorenz-Mie theory, i.e. $Q_{\mathrm{ext}} = Q_{\mathrm{sca}} + Q_{\mathrm{abs}}$
$\mathrm{f}(d_{\mathrm{p}})$	Frequency distribution, for example, Gaussian or Log-normal
A_{dep}	Sample deposition area on the filter
M_{T}	Gravimetric mass (measured or calculated for a known particle size distribution assuming spherical particles)
x	Size parameter, $x = \pi d_{\mathrm{p}}/4$
n_{PS}	Real part of complex refractive index for polystyrene
k_{PS}	Imaginary part of complex refractive index for polystyrene
nQ,o	Real part of complex refractive index for quartz associated with the ordinary ray
$\mathrm{n}_{\mathrm{Q,eo}}$	Real part of complex refractive index for quartz associated with the extra-ordinary ray
$\mathrm{k}_{\mathrm{Q,o}}$	Imaginary part of complex refractive index for quartz associated with the ordinary ray
$\mathrm{k}_{\mathrm{Q,eo}}$	Imaginary part of complex refractive index for quartz associated with the extra-ordinary ray
$M_{\mathrm{T}}/A_{\mathrm{dep}}$	Packing density on filter media
$d_{\mathrm{ve}}^{\mathrm{c}}$	Number-based volume equivalent diameter for a log-normal size distribution

(*continued on next page*)

(*continued*)

Symbol	Description
σ_g	Geometric standard deviation for a log-normal size distribution
b	Bias in mass quantification
$M_{cal}(\epsilon_{Mie})$	Mass of the sampled aerosol with a known size distribution calculated from the SRM calibration curve, $M_{cal} = \epsilon_{Mie}$/Slope

Appendix A. Supplementary data

Supplementary data to this article can be found online at https://doi.org/10.1016/j.jaerosci.2025.106669.

Data availability

The data generated or analyzed during this study can be found within the published article and its supplementary files. Additional data is available from the corresponding author on reasonable request.

References

Ashraf, S., Niskanen, I., Kanyathare, B., Vartiainen, E., Mattsson, C., Heikkilä, R., & Thungström, G. (2019). Determination of complex refractive index of SU-8 by Kramers–Kronig dispersion relation method at the wavelength range 2.5–22.0 μm. *Journal of Quantitative Spectroscopy and Radiative Transfer, 224*, 309–311. https://doi.org/10.1016/j.jqsrt.2018.11.026

ASTM. (2014). ASTM D7948: Standard test method for measurement of respirable crystalline silica in workplace air by infrared spectrometry. https://store.astm.org/d7948-20.html.

Bandopadhyay, A. K. (2010). Determination of quartz content for Indian coals using an FTIR technique. *International Journal of Coal Geology, 81*(1), 73–78. https://doi.org/10.1016/j.coal.2009.10.018

Bartz, H., Franzen, H., & Fissan, H. (1979). Auswertung von Kaskaden- impaktormessungen unter Beriicksich tigung der Wandver-luste und der realen Abscheidekarakteristiken. *Staub Reinhaltung der Luft, 39*, 112–115.

Bhaskar, R., Li, J., & Xu, L. (1994). A comparative study of particle size dependency of IR and XRD methods for quartz analysis. *American Industrial Hygiene Association Journal, 55*(7), 605–609. https://doi.org/10.1080/15428119491018682

Bohren, C. F., & Huffman, D. R. (2008). *Absorption and scattering of light by small particles*. John Wiley & Sons.

Brewster, M. Q., & Tien, C. L. (1982). Radiative transfer in packed/fluidized beds: Dependent Vs. Independent scattering. *American Society of Mechanical Engineers, 104* (November), 573–579 *(Paper)*.

Cares, J. W., Goldin, A. S., Lynch, J. J., & Burgess, W. A. (1973). The determination of quartz in airborne respirable granite dust by infrared speetrophotometry. *American Industrial Hygiene Association Journal, 34*(7), 298–305. https://doi.org/10.1080/0002889738506850

Cartigny, J. D., Yamada, Y., & Tien, C. L. (1986). Radiative transfer with dependent scattering by particles: Part 1—theoretical investigation. *Journal of Heat Transfer, 108*(3), 608–613. https://doi.org/10.1115/1.3246979

Chisholm, J. (1999). Respirable dust and respirable silica concentrations from construction activities. *Indoor and Built Environment, 8*(2), 94–106. https://doi.org/10.1177/1420326X9900800204

Ciddor, P. E. (1996). Refractive index of air: New equations for the visible and near infrared. *Applied Optics, 35*(9), 1566. https://doi.org/10.1364/ao.35.001566

Dekeyser, E., & Dams, R. (1990). Size distribution analysis of cascade impactor and multistage cyclone emission samples by a SEM-based imaging system. *Scanning, 12* (1), 41–48. https://doi.org/10.1002/sca.4950120108

Dempster, P. B., & Ritchie, P. D. (1952). Surface of finely-ground silica. *Nature, 169*(4300), 538–539. https://doi.org/10.1038/169538b0

Di Biagio, C., Boucher, H., Caquineau, S., Chevaillier, S., Cuesta, J., & Formenti, P. (2014). Variability of the infrared complex refractive index of African mineral dust: Experimental estimation and implications for radiative transfer and satellite remote sensing. *Atmospheric Chemistry and Physics, 14*(20), 11093–11116. https://doi.org/10.5194/acp-14-11093-2014

Dodgson, J., & Whittaker, W. (1973). The determination of quartz in respirable dust samples by infrared spectrophotometry–I: The potassium bromide disc method. *Annals of Occupational Hygiene, 16*(4), 373–387. https://doi.org/10.1093/annhyg/16.4.373

Drolen, B. L., & Tien, C. L. (1987). Independent and dependent scattering in packed-sphere systems. *Journal of Thermophysics and Heat Transfer, 1*(1), 63–68. https://doi.org/10.2514/3.8

Dunbar, C., & Mitchell, J. (2005). Analysis of cascade impactor mass distributions. *Journal of Aerosol Medicine: Deposition, Clearance, and Effects in the Lung, 18*(4), 439–451. https://doi.org/10.1089/jam.2005.18.439

Dzubay, T. G., & Hasan, H. (1990). Fitting multimodal lognormal size distributions to Cascade impactor data. *Aerosol Science and Technology, 13*(2), 144–150. https://doi.org/10.1080/02786829008959432

Foster, R. D., & Walker, R. F. (1984). Quantitative determination of crystalline silica in respirable-size dust samples by infrared spectrophotometry. *The Analyst, 109* (9), 1117. https://doi.org/10.1039/an9840901117

Gharpure, A., Heim, J. W., & Vander Wal, R. L. (2021). Characterization and hazard identification of respirable cement and concrete dust from construction activities. *International Journal of Environmental Research and Public Health, 18*(19). https://doi.org/10.3390/ijerph181910126

Gordon, R. L., & Harris, G. W. (1955). Effect of particle-size on the quantitative determination of quartz by X-ray diffraction. *Nature, 175*(4469). https://doi.org/10.1038/1751135a0, 1135–1135.

Hand, J. L., & Kreidenweis, S. M. (2002). A new method for retrieving particle refractive index and effective density from aerosol size distribution data. *Aerosol Science and Technology, 36*(10), 1012–1026. https://doi.org/10.1080/02786820290092276

Hänel, G. (1968). The real part of the mean complex refractive index and the mean density of samples of atmospheric aerosol particles. *Tellus, 20*(3), 371–379. https://doi.org/10.1111/j.2153-3490.1968.tb00378.x

Hanssen, L. M., & Zhu, C. (2002). Wavenumber standards for mid-infrared spectrometry. In J. M. Chalmers, & P. R. Griffiths (Eds.), *Handbook of vibrational spectroscopy* (pp. 881–890). John Wiley & Sons Ltd. https://doi.org/10.1002/0470027320.s0701.

Hapke, B. (2012). *Theory of reflectance and emittance spectroscopy*. Cambridge University Press. https://doi.org/10.1017/CBO9781139025683

Harrick, N. J., & Riederman, N. H. (1965). Infrared spectra of powders by means of internal reflection spectroscopy. *Spectrochimica Acta, 21*(12), 2135–2139. https://doi.org/10.1016/0371-1951(65)80229-6

Hasan, H., & Dzubay, T. G. (1983). Apportioning light extinction coefficients to chemical species in atmospheric aerosol. *Atmospheric Environment, 17*(8), 1573–1581. https://doi.org/10.1016/0004-6981(83)90310-4

He, M., Yan, W., Chang, Y., Liu, K., & Liu, X. (2019). Fundamental infrared absorption features of α-quartz: An unpolarized single-crystal absorption infrared spectroscopic study. *Vibrational Spectroscopy, 101*, 52–63. https://doi.org/10.1016/j.vibspec.2019.02.003. January.

Hottel, H. C., Sarofim, A. F., Dalzell, W. H., & Vasalos, I. A. (1971). Optical properties of coatings. Effect of pigment concentration. *AIAA Journal, 9*(10), 1895–1898. https://doi.org/10.2514/3.49999

Hudson, P. K., Young, M. A., Kleiber, P. D., & Grassian, V. H. (2008). Coupled infrared extinction spectra and size distribution measurements for several non-clay components of mineral dust aerosol (quartz, calcite, and dolomite). *Atmospheric Environment, 42*(24), 5991–5999. https://doi.org/10.1016/j.atmosenv.2008.03.046

Hunt, G. R., & Logan, L. M. (1972). Variation of single particle mid-infrared emission spectrum with particle size. *Applied Optics, 11*(1), 142. https://doi.org/10.1364/ao.11.000142

Ishimaru, A., & Kuga, Y. (1982). Attenuation constant of a coherent field in a dense distribution of particles. *Journal of the Optical Society of America, 72*(10), 1317–1320. https://doi.org/10.1364/josa.72.001317

Jäger, C., Il'in, V. B., Henning, T., Mutschke, H., Fabian, D., Semenov, D. A., & Voshchinnikov, N. V. (2003). A database of optical constants of cosmic dust analogs. *Journal of Quantitative Spectroscopy and Radiative Transfer, 79–80*, 765–774. https://doi.org/10.1016/S0022-4073(02)00301-1

Jung, M. R., Horgen, F. D., Orski, S. V., Rodriguez, C. V., Beers, K. L., Balazs, G. H., Jones, T. T., Work, T. M., Brignac, K. C., Royer, S. J., Hyrenbach, K. D., Jensen, B. A., & Lynch, J. M. (2018). Validation of ATR FT-IR to identify polymers of plastic marine debris, including those ingested by marine organisms. *Marine Pollution Bulletin, 127*(November 2017), 704–716. https://doi.org/10.1016/j.marpolbul.2017.12.061

Kauffer, E., Moulut, J. C., Masson, A., Protois, J. C., & Grzebyk, M. (2002). Comparison by X-ray diffraction and infrared spectroscopy of two samples of α quartz with the NIST SRM 1878a α quartz. *Annals of Occupational Hygiene, 46*(4), 409–421. https://doi.org/10.1093/annhyg/mef050

Kischkat, J., Peters, S., Gruska, B., Semtsiv, M., Chashnikova, M., Klinkmüller, M., Fedosenko, O., MacHulik, S., Aleksandrova, A., Monastyrskyi, G., Flores, Y., & Masselink, W. T. (2012). Mid-infrared optical properties of thin films of aluminum oxide, titanium dioxide, silicon dioxide, aluminum nitride, and silicon nitride. *Applied Optics, 51*(28), 6789–6798. https://doi.org/10.1364/AO.51.006789

Koopmans, K., & Rieck, G. D. (1965). On the thickness of the disturbed layer on ground quartz powder with particle size of 1 5 m. *British Journal of Applied Physics, 16*(12), 1913–1914. https://doi.org/10.1088/0508-3443/16/12/418

Ku, B. K., Deye, G., & Turkevich, L. A. (2013). Characterization of a vortex shaking method for aerosolizing fibers. *Aerosol Science and Technology, 47*(12), 1293–1301. https://doi.org/10.1080/02786826.2013.836588

Larsen, D. J., von Doenhoff, L. J., & Crable, J. V. (1972). The quantitative dermination of quartz in coal dust by infrared spectroscopy. *American Industrial Hygiene Association Journal, 33*(6), 367–372. https://doi.org/10.1080/0002889728506666

Liu, Y., & Daum, P. H. (2008). Relationship of refractive index to mass density and self-consistency of mixing rules for multicomponent mixtures like ambient aerosols. *Journal of Aerosol Science, 39*(11), 974–986. https://doi.org/10.1016/j.jaerosci.2008.06.006

Longtin, D. R., Shettle, E. P., Hummel, J. R., & Pryce, J. D. (1988). *A wind dependent desert aerosol dust model: Radiative properties*. Afgl-Tr-88-0112.

Lowenthal, D. H., Watson, J. G., & Saxena, P. (2000). Contributions to light extinction during project MOHAVE. *Atmospheric Environment, 34*(15), 2351–2359. https://doi.org/10.1016/S1352-2310(99)00449-5

Lukacs, R., Blümel, R., Zimmerman, B., Bałciołlu, M., & Kohler, A. (2015). Recovery of absorbance spectra of micrometer-sized biological and inanimate particles. *Analyst, 140*(9), 3273–3284. https://doi.org/10.1039/c5an00401b

Madsen, F. A., Rose, M. C., & Cee, R. (1995). Review of quartz analytical methodologies: Present and future needs. *Applied Occupational and Environmental Hygiene, 10*(12), 991–1002. https://doi.org/10.1080/1047322X.1995.10389086

Marple, V. A., Rubow, K. L., & Behm, S. M. (1991). A microorifice uniform deposit impactor (MOUDI): Description, calibration, and use. *Aerosol Science and Technology, 14*(4), 434–446. https://doi.org/10.1080/02786829108959504

Mathar, R. J. (2007). Refractive index of humid air in the infrared: Model fits. *Journal of Optics A: Pure and Applied Optics, 9*(5), 1–8. https://doi.org/10.1088/1464-4258/9/5/008

Mätzler, C. (2002). *MATLAB functions for Mie scattering and absorption*. https://doi.org/ResearchReportNo.2002-08.

McCallion, O. N. M., Taylor, K. M. G., Bridges, P. A., Thomas, M., & Taylor, A. J. (1996). Jet nebulisers for pulmonary drug delivery. *International Journal of Pharmaceutics, 130*(1), 1–11. https://doi.org/10.1016/0378-5173(95)04233-4

Menzelintseva, N., Karapuzova, N., Redhwan, A. M., & Fomina, E. (2019). Study of dust particle size distribution in the air of work areas at cement production facilities. In *E3S web of conferences* (Vol. 138, pp. 0–6). https://doi.org/10.1051/e3sconf/201913801027

Occupational respiratory diseases. In Merchant, J. A., Boehlecke, B. A., Taylor, G., & Pickett-Harner, M. (Eds.), *DHHS (NIOSH) (Issue Publication No. 86-102)*, (1986). https://doi.org/10.26616/NIOSHPUB86102

Mie, G. (1908). Beiträge zur Optik trüber Medien, speziell kolloidaler Metallösungen. *Annalen der Physik, 330*(3), 377–445. https://doi.org/10.1002/andp.19083300302

MSHA. (2013). Infrared determination of quartz in respirable coal mine dust: Method P-7. *Mine Safety and Health Division, Pittsburgh Safety and Health Technology Center*, 1–18. https://arlweb.msha.gov/Techsupp/pshtcweb/MSHAP7.pdf.

Myers, T. L., Tonkyn, R. G., Danby, T. O., Taubman, M. S., Bernacki, B. E., Birnbaum, J. C., Sharpe, S. W., & Johnson, T. J. (2018). Accurate measurement of the optical constants n and k for a series of 57 inorganic and organic liquids for optical modeling and detection. *Applied Spectroscopy, 72*(4), 535–550. https://doi.org/10.1177/0003702817742848

Nagelschmidt, G., Gordon, R. L., & Griffin, O. G. (1952). Surface of finely-ground silica. *Nature, 169*(4300), 539–540. https://doi.org/10.1038/169539a0

NIOSH. (2017a). Nmam 7603: Quartz in respirable coal mine dust, by IR (Redeposition). *NIOSH Manual of Analytical Methods (NMAM), Fifth Edition, 4*, 2–9. https://www.cdc.gov/niosh/nmam/pdf/7603.pdf.

NIOSH. (2017b). Silica, respirable crystalline by IR (KBr pellet): Method 7602. *NIOSH Manual of Analytical Methods (NMAM), 4*, 1–7.

OSHA. (2016). Occupational exposure to respirable crystalline silica, final rule. *Federal Registers, 81*, 16285–16890. https://www.osha.gov/laws-regs/federalregister/2016-03-25-1.

Ouimette, J. R., & Flagan, R. C. (1982). The extinction coefficient of multicomponent aerosols. *Atmospheric Environment, 16*(10), 2405–2419. https://doi.org/10.1016/0004-6981(82)90131-7

Page, S. J. (2003). Comparison of coal mine dust size distributions and calibration standards for crystalline silica analysis. *American Industrial Hygiene Association Journal, 64*(1), 30–39. https://doi.org/10.1080/15428110308984781

Pan, L., Golden, S., Assemi, S., Sime, M. F., Wang, X., Gao, Y., & Miller, J. (2021). Characterization of particle size and composition of respirable coal mine dust. *Minerals, 11*(3), 1–12. https://doi.org/10.3390/min11030276

Pavan, C., Polimeni, M., Tomatis, M., Corazzari, I., Turci, F., Ghigo, D., & Fubini, B. (2016). Abrasion of artificial stones as a new cause of an ancient disease. Physicochemical features and cellular responses. *Toxicological Sciences, 153*(1), 4–17. https://doi.org/10.1093/toxsci/kfw101

Peterson, J. T., & Weinman, J. A. (1969). Optical properties of quartz dust particles at infrared wavelengths. *Journal of Geophysical Research, 74*(28), 6947–6952. https://doi.org/10.1029/JC074i028p06947

Polyanskiy, M. N. (2024). Refractiveindex.info database of optical constants. *Scientific Data, 11*(1), 1–19. https://doi.org/10.1038/s41597-023-02898-2

Querry, M. R. (1985). Optical constants. *Report No. CRDC-CD-85034* https://apps.dtic.mil/sti/pdfs/ADA158623.pdf.

Querry, M. (1987). Optical constants of minerals and other materials from the millimeter to the ultraviolet. Report No. CRDEC-CD-88009 https://apps.dtic.mil/sti/pdfs/ADA192210.pdf.

Ramkissoon, C., Gaskin, S., Hall, T., Pisaniello, D., & Zosky, G. (2023). Engineered stone fabrication work releases volatile organic compounds classified as lung irritants. *Annals of Work Exposures and Health, 67*(2), 288–293. https://doi.org/10.1093/annweh/wxac068

Ramkissoon, C., Gaskin, S., Thredgold, L., Hall, T., Rowett, S., & Gun, R. (2022). Characterisation of dust emissions from machined engineered stones to understand the hazard for accelerated silicosis. *Scientific Reports, 12*(1), 4351. https://doi.org/10.1038/s41598-022-08378-8

Rank, D. H., & Shearer, J. N. (1954). Index of refraction of air in the infrared. *Journal of the Optical Society of America, 44*(7), 575. https://doi.org/10.1364/JOSA.44.000575

Rappaport, S. M., Goldberg, M., Susi, P., & Herrick, R. F. (2003). Excessive exposure to silica in the US construction industry. *Annals of Occupational Hygiene, 47*(2), 111–122. https://doi.org/10.1093/annhyg/meg025

Reed, B. E., Peters, D. M., McPheat, R., Smith, A. J. A., & Grainger, R. G. (2017). Mass extinction spectra and size distribution measurements of quartz and amorphous silica aerosol at 0.33–19 μm compared to modelled extinction using Mie, CDE, and T-matrix theories. *Journal of Quantitative Spectroscopy and Radiative Transfer, 199*, 52–65. https://doi.org/10.1016/j.jqsrt.2017.05.011

Rice, F. L., Key-Schwartz, R., Bartley, D., Baron, P., & Schlecht, P. (2002). Health effects of occupational exposure to respirable crystalline silica. *NIOSH hazard review*. DHHS (NIOSH) Publication No. 2002-129. www.cdc.gov/niosh.

Riley, K. W., French, D. H., Farrell, O. P., Wood, R. A., & Huggins, F. E. (2012). Modes of occurrence of trace and minor elements in some Australian coals. *International Journal of Coal Geology, 94*, 214–224. https://doi.org/10.1016/j.coal.2011.06.011

Rishi, K., Ku, B. K., Qi, C., Thompson, D., Wang, C., Dozier, A., Vogiazi, V., Zervaki, O., & Kulkarni, P. (2024). Release of crystalline silica nanoparticles during engineered stone fabrication. *ACS Omega, 9*(51), 50308–50317. https://doi.org/10.1021/acsomega.4c06437

Saksena, B. D. (1940). Analysis of the Raman and infra-red spectra of α-quartz. *Proceedings of the Indian Academy of Sciences - Section A, 12*(1), 93–139. https://doi.org/10.1007/BF03170730

Saksena, B. D. (1958). The infra-red absorption spectra of α-quartz between 4 and 15 microns. *Proceedings of the Physical Society, 72*(1), 9–16. https://doi.org/10.1088/0370-1328/72/1/303

Sato, K., Kurosawa, F., & Kammori, O. (1969). Effect of particle size on infrared spectra of inorganic powders. *Bulletin of the Chemical Society of Japan, 42*(12), 3593–3596. https://doi.org/10.1246/bcsj.42.3593

Silva, L. S., Amario, M., Stolz, C. M., Figueiredo, K. V., & Haddad, A. N. (2023). A comprehensive review of stone dust in concrete: Mechanical behavior, durability, and environmental performance. *Buildings, 13*(7). https://doi.org/10.3390/buildings13071856

Šimon, I., & McMahon, H. O. (1953). Study of the structure of quartz, cristobalite, and vitreous silica by reflection in infrared. *The Journal of Chemical Physics, 21*(1), 23–30. https://doi.org/10.1063/1.1698615

Sirianni, G., Hosgood, H. D., Slade, M. D., & Borak, J. (2008). Particle size distribution and particle size-related crystalline silica content in granite quarry dust. *Journal of Occupational and Environmental Hygiene, 5*(5), 279–285. https://doi.org/10.1080/15459620801947259

Smith, W. R., & Henderson, D. (1970). Analytical representation of the Percus-Yevick hard-sphere radial distribution function. *Molecular Physics, 19*(3), 411–415. https://doi.org/10.1080/00268977000101421

Song, Y., Southam, K., Beamish, B. B., & Zosky, G. R. (2022). Effects of chemical composition on the lung cell response to coal particles: Implications for coal workers' pneumoconiosis. *Respirology, 27*(6), 447–454. https://doi.org/10.1111/resp.14246

Sosa, J. M., Huber, D. E., Welk, B., & Fraser, H. L. (2014). Development and application of MIPAR™: A novel software package for two- and three-dimensional microstructural characterization. *Integrating Materials and Manufacturing Innovation, 3*(1), 123–140. https://doi.org/10.1186/2193-9772-3-10

Spitzer, W. G., & Kleinman, D. A. (1961). Infrared lattice bands of quartz. *Physical Review, 121*(5), 1324–1335. https://doi.org/10.1103/PhysRev.121.1324

Stacey, P., Kauffer, E., Moulut, J. C., Dion, C., Beauparlant, M., Fernandez, P., Key-Schwartz, R., Friede, B., & Wake, D. (2009). An international comparison of the crystallinity of calibration materials for the analysis of respirable α-quartz using X-ray diffraction and a comparison with results from the infrared KBr disc method. *Annals of Occupational Hygiene, 53*(6), 639–649. https://doi.org/10.1093/annhyg/mep038

Steyer, T. R., Day, K. L., & Huffman, D. R. (1974). Infrared absorption by small amorphous quartz spheres. *Applied Optics, 13*(7), 1586. https://doi.org/10.1364/ao.13.001586

Sumlin, B. J., Heinson, W. R., & Chakrabarty, R. K. (2018). Retrieving the aerosol complex refractive index using PyMieScatt: A Mie computational package with visualization capabilities. *Journal of Quantitative Spectroscopy and Radiative Transfer, 205*, 127–134. https://doi.org/10.1016/j.jqsrt.2017.10.012

Thompson, D., & Qi, C. (2023). Characterization of the emissions and crystalline silica content of airborne dust generated from grinding natural and engineered stones. *Annals of Work Exposures and Health, 67*(2), 266–280. https://doi.org/10.1093/annweh/wxac070

Tuddenham, W. M., & Lyon, R. J. P. (1960). Infrared techniques in the identification and measurement of minerals. *Analytical Chemistry, 32*(12), 1630–1634. https://doi.org/10.1021/ac60168a026

Twersky, V. (1978). Acoustic bulk parameters in distributions of pair-correlated scatterers. *Journal of the Acoustical Society of America, 64*(6), 1710–1719. https://doi.org/10.1121/1.382150

Udvardi, B., Kovács, I. J., Fancsik, T., Kónya, P., Bátori, M., Stercel, F., Falus, G., & Szalai, Z. (2017). Effects of particle size on the attenuated total reflection spectrum of minerals. *Applied Spectroscopy, 71*(6), 1157–1168. https://doi.org/10.1177/0003702816670914

Verma, D. K., Sebestyen, A., Julian, J. A., & Muir, D. C. F. (1992). A comparison of two methods of sampling and analysis for free crystalline silica α-Quartz. *Applied Occupational and Environmental Hygiene, 7*(11), 758–763. https://doi.org/10.1080/1047322X.1992.10388083

Verma, D. K., & Shaw, D. S. (2001). A comparison of international silica (α-quartz) calibration standards by fourier transform-infrared spectrophotometry. *Annals of Occupational Hygiene, 45*(6), 429–435. https://doi.org/10.1016/S0003-4878(00)00083-1

Virji, M. A., Bello, D., Woskie, S. R., Liu, X. M., & Kalil, A. J. (2002). Analysis of quartz by FT-IR in air samples of construction dust. *Applied Occupational and Environmental Hygiene, 17*(3), 165–175. https://doi.org/10.1080/104732202753438252

Wang, X., Abbasi, B., Elahifard, M., Osho, B., Chen, L. W. A., Chow, J. C., & Watson, J. G. (2024). Coal mine dust size distributions, chemical compositions, and source apportionment. *Minerals, 14*(11). https://doi.org/10.3390/min14111122

Wenrich, M. L., & Christensen, P. R. (1996). Optical constants of minerals derived from emission spectroscopy: Application to quartz. *Journal of Geophysical Research: Solid Earth, 101*(B7), 15921–15931. https://doi.org/10.1029/96JB01153

Wertheim, M. S. (1963). Exact solution of the percus-yevick integral equation for hard spheres. *Physical Review Letters, 10*(8), 321–323. https://doi.org/10.1103/PhysRevLett.10.321

Yamada, Y., Cartigny, J. D., & Tien, C. L. (1986). Radiative transfer with dependent scattering by particles: Part 2—Experimental investigation. *Journal of Heat Transfer, 108*(3), 614–618. https://doi.org/10.1115/1.3246980